Entanglement from Sky: Optimizing Satellite-based Entanglement Distribution for Quantum Networks

Xinliang Wei, *Member, IEEE*, Lei Fan, *Senior Member, IEEE*, Yuanxiong Guo, *Senior Member, IEEE*, Zhu Han, *Fellow, IEEE* and Yu Wang, *Fellow, IEEE*

***Abstract*—The advancement of satellite-based quantum networks shows promise in transforming global communication infrastructure by establishing a secure and reliable quantum Internet. These networks use optical signals from satellites to ground stations to distribute high-fidelity quantum entanglements over long distances, overcoming the limitations of traditional terrestrial systems. However, the complexity of satellite-based entanglement distribution and terrestrial quantum swapping in the integrated network requires joint optimization with satellite assignment, resource allocation, and path selection. To address this challenge, we introduce a hybrid quantum-classical algorithm to solve the optimization problem by leveraging the strengths of both quantum and classical computing. The original problem is decomposed into a master problem and several subproblems using Dantzig-Wolfe decomposition and linearization techniques. Through experiments, this study demonstrates the effectiveness and reliability of the proposed methods in optimizing large-scale networks and managing qubit usage compared to the classical optimization techniques. The findings provide valuable insights for designing and implementing satellite-based entanglement distribution in quantum networks, paving the way for a secure global quantum communication infrastructure.**

***Index Terms*—Entanglement distribution, quantum swapping, quantum networks, hybrid quantum-classical optimization, space-terrestrial integrated network**

I. Introduction

QUANTUM entanglement distribution has the potential to revolutionize fields such as quantum secure communication [1], quantum key distribution (QKD) [2], and quantum teleportation (QT) [3]. However, it has been a challenge to distribute quantum entanglement in the development of quantum networks. Ground-based methods have faced limitations and drawbacks that hinder their effectiveness. These limitations include susceptibility to environmental disturbances such as atmospheric interference and fiber attenuation, which can degrade the fidelity of entangled states and limit the achievable distances for entanglement distribution. Moreover, ground-based systems are also vulnerable to eavesdropping, posing a significant security risk for quantum communication.

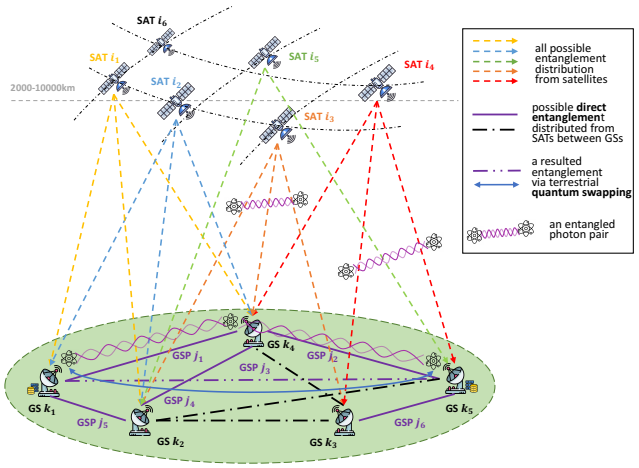

Fig. 1. The overall satellite-based entanglement distribution and terrestrial quantum swapping architecture.

In recent years, there has been increasing interest in utilizing satellite-based quantum entanglement distribution as an alternative approach, as depicted in Fig. 1. This method offers several advantages over ground-based techniques by leveraging space-based platforms. Satellite-based distribution can overcome environmental factors that typically degrade entanglement fidelity on the ground, enabling the establishment of long-distance entangled links with enhanced fidelity and security. Furthermore, the ability to distribute entangled states from space enables global coverage, overcoming the geographical limitations of ground-based systems. The architecture of a satellite-based quantum network typically involves deploying quantum-enabled satellites equipped with entangled photon sources and communication modules, serving as relay nodes to distribute entangled states between ground stations equipped with photon receivers, thereby creating a global-scale quantum network. This satellite-based infrastructure facilitates the establishment of quantum links between geographically distant locations, enabling secure communication and quantum key distribution on a global scale [4]–[6].

Despite the promising potential of satellite-based quantum entanglement distribution, previous studies [7]–[9] have encountered several limitations and challenges. For instance, Khatri *et al.* [7] extensively investigated the double downlink architecture for a satellite constellation in polar orbits,

X. Wei and Y. Wang are with the Department of Computer and Information Sciences, Temple University, Philadelphia, PA 19112. {xinliang.wei, wangyu}@temple.edu. L. Fan is with the Department of Engineering Technology and Department of Electrical and Computer Engineering at the University of Houston, Houston, TX 77004. lfan8@central.uh.edu. Y. Guo is with the Department of Information Systems and Cyber Security, University of Texas at San Antonio, San Antonio, TX 78249. yuanxiong.guo@utsa.edu. Z. Han is with the Department of Electrical and Computer Engineering at the University of Houston, Houston, TX 77004 USA, and also with the Department of Computer Science and Engineering, Kyung Hee University, Seoul, South Korea, 446-701. hanzhu22@gmail.com. X. Wei and Y. Wang are the co-corresponding authors. The work is partially supported by the US NSF (Grant No. CNS-2006604, CNS-2106761, CNS-2107216, CNS-2128368, CNS-2128378, CNS-2318663, CMMI-2222670, CMMI-2222810, and ECCS-2302469), the US Department of Transportation, Toyota, Amazon, and Japan Science and Technology Agency (JST) Adopting Sustainable Partnerships for Innovative Research Ecosystem (ASPIRE) under JPMJAP2326.

aiming to optimize entanglement distribution rates between ground stations by reducing the number of deployed satellites. However, their approach which is based on a heuristic greedy algorithm, overlooked certain resource constraints in the problem formulation, such as the number of transmitters and receivers. Similarly, Panigrahy *et al.* [8] considered resource constraints at satellites and ground stations but efficiently solved the problem only for specific scenarios by transforming it into maximum weight independent set or maximum weight bipartite matching problems. Therefore, a more versatile approach is necessary, such as incorporating terrestrial quantum swapping to support satellite-based quantum entanglement distribution scenarios.

Given the limited resources in satellite-based quantum networks, including the number of transmitters per satellite, photon sources, and receivers at ground stations, it is crucial to allocate network resources and schedule transmissions efficiently. This optimization is essential for enhancing network performance while considering the specific satellite constellation and ground station configurations. In this study, we explore a scenario involving joint satellite assignment, resource allocation, and path selection to establish quantum entanglements for ground stations using satellite-based entanglement distribution and terrestrial quantum swapping within the space-terrestrial integrated network (STIN). By integrating terrestrial quantum swapping into satellite-based distribution, more traffic ground station pairs can be accommodated, leading to improved quantum entanglement for various quantum applications. We introduce a joint optimization model and a novel hybrid quantum-classical Dantzig-Wolfe (HQCDW) decomposition technique, combining the strengths of quantum and classical computing to effectively manage network resources in a large-scale setting. Our proposed methodologies aim to address the limitations of existing approaches and tackle the challenges associated with satellite-based entanglement distribution and quantum communication, with the ultimate goal of enabling global-scale quantum communication and computation, thereby unlocking the full potential of quantum technologies for secure and efficient information processing.

To sum up, the contributions of this paper are as follows.

- We explore a scenario of distributing entanglement via both satellites and terrestrial quantum swapping to cooperatively generate entanglement for pairs of traffic ground stations. We formulate a joint satellite assignment, resource allocation, and path selection problem modeled as integer non-linear programming (INLP), to maximize the overall utility of all traffic ground station pairs.
- We propose a novel hybrid quantum-classical Dantzig-Wolfe decomposition algorithm (HQCDW) by leveraging the advantage of both quantum and classical computing to solve the complex INLP problem. The original optimization problem is decomposed into a master problem that is solved in a classical computer and several subproblems that are processed in a quantum annealer. Several linearization strategies are proposed to handle the qubit limitation for different network scales.
- We conduct extensive simulations using the commercial quantum annealer to evaluate our proposed algorithms. Numerous experiments have demonstrated that our proposed HQCDW can handle more complex network settings compared to the non-decomposed manner, and achieve the same result as the classical schemes but with shorter solver accessing time, which demonstrates the quantum advantage.

The remainder of this paper is structured as follows. Section II reviews related work. Section III introduces our system model and the joint optimization problem is formulated in Section IV. Section V presents our proposed methodologies HQCDW and several linearization strategies. Evaluations of the proposed method are provided in Section VI and Section VII concludes the paper with possible future directions. A preliminary version of this paper appears as [10].

II. Related Work

Entanglement Distribution: A long-standing subject of Yin *et al.* [11] is to transfer a quantum state over arbitrary distances. Being of fundamental interest, the result represented a significant step towards a global quantum network. Yin *et al.* [4] demonstrated the satellite-based distribution of entangled photon pairs to two locations separated by 1203 kilometers on Earth. Wang *et al.* [5] explored using orbital angular momentum (OAM) for satellite-based entanglement distribution, showing potential for improved loss-distance scaling. Yin *et al.* [6] demonstrated entanglement-based QKD between two ground stations separated by 1,120 kilometers at a finite secret-key rate of 0.12 bits per second, without the need for trusted relays. Khatri *et al.* [7] proposed a global-scale quantum Internet consisting of a constellation of orbiting satellites that provides a continuous, on-demand entanglement distribution service to ground stations. Following a similar scenario, Panigrahy *et al.* [8] solved it efficiently for some special cases. Wei *et al.* [9] further proposed a few solutions for more different cases. Liorni *et al.* [12] proposed to combine quantum repeaters and satellite-based links, into a scheme that allows achieving entanglement distribution over global distances with a small number of intermediate untrusted nodes. Gonzalez-Raya *et al.* [13] studied the effects of atmospheric turbulence in continuous-variable entanglement distribution and quantum teleportation in the optical regime between a ground station and a satellite. Chang *et al.* [14] defined a system model that considers both satellite movement over time and inter-satellite links. Previous research has largely focused on verifying the possibility of satellite-based entanglement without taking into account practical resource limitations or addressing only special cases. Additionally, terrestrial quantum swapping has been overlooked in previous studies. Our work, however, takes into consideration a broader range of scenarios and specific resource constraints and introduces terrestrial quantum swapping when distributing entanglement via satellite.

Quantum Computing for Optimization: Quantum computing (QC) has been proven to be superior to solving many challenging computationally intensive problems [15]–[19]. For example, Jeong *et al.* [15] introduced quantum-inspired binary particle swarm optimization (QBPSO), combining conventional BPSO with quantum computing principles. Glover *et al.* [16] discussed the features of the quadratic unconstrained

binary optimization (QUBO) model, highlighting its broad applications in optimization. Ajagekar *et al.* [17] explored quantum computing applications in energy systems optimization and addressed associated challenges. Borders *et al.* [18] demonstrated integer factorization as an example of problems addressed by adiabatic and gated quantum computing. Tilly *et al.* [19] aimed to provide an overview of the progress made on various parts of the algorithm. Recently, a hybrid quantum-classical (HQC) computing framework has been developed to solve complex optimization problems using both quantum and classical computers, as the current state of quantum computers is limited by availability and cost. Such hybrid quantum optimization has been applied in different areas including machine learning, mobile computing, network communication, and task scheduling [20]–[28]. For instance, Tran *et al.* [20] first introduced an HQC approach for solving the complete tree search problem, while Ajagekar *et al.* [24] proposed HQC-based optimization techniques for large-scale scheduling problems. Similarly, both [23] and [25] developed HQC algorithms using Benders' decomposition techniques to solve mixed integer linear programming (MILP) problems. Such a method has been applied in distributed learning [27], [29]. Zhao et al. [26] further employed a quantum approximate optimization algorithm (QAOA) to assist in solving the master problem within the Benders' decomposition framework. Paterakis [22] also provided an HQC optimization algorithm for unit commitment problems and introduced a method for controlling the size of the master problem through various cut selection criteria. Similar to previous studies, our works also utilize the HQC computing framework but leverage the Dantzig-Wolfe (DW) decomposition technique based on the nature of our formulated problem.

III. System Model

A. Space-Terrestrial Integrated Network (STIN)

We consider a STIN that consists of $|M|$ satellites (SAT), $|N|$ ground stations (GS), and total $|O|$ ground station pairs (GSP) as shown in Fig. 1, where $M = \{1, \cdots, |M|\}$ indexed by i, $N = \{1, \cdots, |N|\}$ indexed by k, $O = \{1, \cdots, |O|\}$ indexed by j. We also define $O' \subseteq O$ as the traffic GSP set that needs to generate the entanglement link. In addition, let $O_k \subset O$ be the GSP set of GS k. We consider the polar satellite constellation and assume that each satellite has a quantum memory that can store at most sm_i entangled photon pairs. Each satellite is also equipped with tr_i transmitters that can transmit entangled photon pairs to multiple GSPs. Let $sm = \{sm_1, sm_2, \cdots, sm_{|M|}\}$ be the quantum memory set of all satellites and we can find the maximal one $sm_{max} = \max\{sm_i, \forall i \in M\}$. Each GS also has a quantum memory gm_k for any quantum application such as QKD or QT. Additionally, each GS owns rr_k receivers to receive the photon from the satellite or generate the entanglement link from other GSs by using quantum swapping. We also define an elevation angle threshold θ_e for any satellite and GSP. The entangled photon can be successfully received at the GS as long as the elevation angle between the satellite and the horizon at the GS exceeds this threshold.

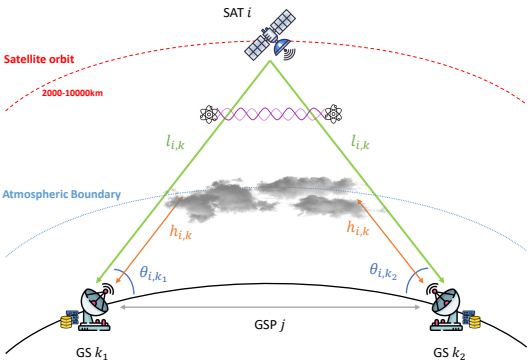

Fig. 2. An example of the space-to-ground transmittance between one SAT and two GSs for the entanglement distribution to this GSP.

B. Loss and Noise Model

The successful distribution of entangled photons through satellite links heavily relies on photonic sources that produce entangled pairs and free-space optical communication strategies. The positioning and organization of these sources, links, and related hardware are dictated by the selected quantum link configuration of the user(s).

In a STIN, there are typically multiple quantum communication paths as illustrated in [13], such as downlink and uplink channels, between a ground station and a satellite, either directly or through an intermediate station. Moreover, there may be lateral paths between two ground stations or two satellites. This work mainly focuses on the dual downlink architecture for photonic entanglement distribution with spontaneous parametric down-conversion (SPDC) [30]. Free-space optical transmission is a crucial aspect to consider in analyzing such links. Therefore, we take into account the optical channel's characteristics, including transmission loss and noise. The transmission of photons from satellites to ground stations can be effectively modeled using a bosonic pure-loss channel with transmittance. Based on previous works [7], [8], the space-to-ground transmittance $\eta_{i,k}^{sg}$ between SAT i and GS k consists of two parts: the free-space transmittance $\eta_{i,k}^{fs}$ and the atmospheric transmittance $\eta_{i,k}^{atm}$, and can be defined as below

$$\eta_{i,k}^{sg} = \eta_{i,k}^{fs} \cdot \eta_{i,k}^{atm}. \tag{1}$$

Here, $\eta_{i,k}^{fs}$ depends on the orbital parameters, such as altitude and zenith angle, while $\eta_{i,k}^{atm}$ depends on the atmospheric conditions, e.g., turbulence and weather conditions. As shown in Fig. 2, let $l_{i,k}$ be the distance length between SAT i and GS k, and $h_{i,k}$ be the distance height between GS k and atmospheric boundary when connected to SAT i. In our analysis, we take into account the circular apertures of diameter d_i^T and d_k^R for the transmitter and receiver telescopes at SAT i and GS k, respectively. These telescopes operate at a specific wavelength λ. Hence, the free-space transmittance and the atmospheric transmittance can be calculated by

$$\eta_{i,k}^{fs} = \frac{(\pi(d_i^T/2)^2)(\pi(d_k^R/2)^2)}{(\lambda l_{i,k})^2}, \quad \eta_{i,k}^{atm} = e^{-\hat{\alpha} h_{i,k}}, \tag{2}$$

where $\hat{\alpha}$ is the atmospheric extinction coefficient.

Next, we examine the transmission of photons in the presence of background photons. Let $\bar{n}_k$ be the number of

background photons received by GS k and F_0 be the initial fidelity of the entangled photon pair. We consider an initially imperfect Bell state under the high-loss low-noise regime with the assumption that $\eta^{sg}_{i,k_1} = \eta^{sg}_{i,k_2} = \eta^{sg}_{i,j}$ and $\bar{n}_{k_1} = \bar{n}_{k_2} = \bar{n}_j$. Therefore, the fidelity of entangled photon pair after transmission can be approximated by

$$F_{i,j} = \begin{cases} \frac{1}{4}\left(1 + \frac{4F_0-1}{(1+\frac{\bar{n}_j}{\eta^{sg}_{i,j}})^2}\right), \text{if } \theta_{i,k_1}, \theta_{i,k_2} \geq \theta_e, (k_1,k_2) \in j, \\ 0, \quad \text{otherwise.} \end{cases} \tag{3}$$

C. Terrestrial Quantum Swapping

An intermediate GS, equipped with quantum memories entangled with memories on two remote GSs, is used to perform entanglement swapping. The successful execution of this process creates an extended entanglement "link" between the remote GSs. The probability of a successful entanglement swapping is represented by ps, while the probability of failure is denoted by $1 - ps$. If the process fails, the two Bell pairs involved are discarded. We consider a perfect quantum swapping and two depolarized Bell states (Werner states) will be swapped to a new Werner state. Then the fidelities of the new states after swapping are defined below [31]–[33]

$$F_{sw} = F_1 F_2 + \frac{(1-F_1)(1-F_2)}{3}, \tag{4}$$

where F_1 and F_2 are the fidelities of two entanglement links, respectively. Note that by considering terrestrial quantum swapping, our entanglement distribution can serve more GSPs (even serving some GSPs which cannot be served by any SAT directly due to either visibility or fidelity issues).

IV. Problem Formulation

The goal of this paper is to solve a joint satellite assignment, resource allocation, and path selection problem for entanglement distribution in STIN. In this problem, each satellite acts as an entangled photon source (EPS) and distributes entangled photon pairs to the GSP. The objective is to maximize the overall utility of all traffic GSPs by optimally assigning the satellites and allocating photon resources to the GSP when a satellite is visible to both GSs within the same GSP.

In cases where no satellite is visible to the GSP, we explore ground-based quantum swapping using the entanglement links generated by satellite-based entanglement distribution. Moreover, we need to determine the optimal path selection for the remaining GSPs. As shown in Fig. 3, given all GSPs, we need to generate an entanglement link for each traffic GSP $j \in O'$ by using either the satellite-based entanglement distribution or terrestrial quantum swapping. Based on the fidelity calculation in Section III-C, we can predict which satellite can be assigned to which GSP and form an entanglement distribution graph (Fig. 3(b)) with both satellite-based assignment (line-dot edges) and quantum swapping (line-dot-dot edges).

Specifically, we are interested in two-hop quantum swapping and denote P as all two-hop paths from the graph indexed by p. Let $R^{gsp}_{p,j} = \{j_1, j_2\}$ be the GSP set in path p for GSP j, and $R^{sat}_{p,j} = \{i_1, i_2\}$ be the related satellite set in path p for GSP j. Moreover, let $P_k \subset P$ be the path set of GS k, $P_j \subset P$ be the path set of GSP j, and $P_i \subset P$ be the path set of SAT i. Denote $w_{i,j}$ as the weight or utility associated with the assignment of SAT i to GSP j and $w_{p,j}$ as the utility associated with the selection of path p for GSP j. We also assume that each satellite can generate at most sm_i entangled photon pairs.

Decision Variables. Let $x_{i,j}$ be a binary variable to indicate whether satellite i ($i \in M$) is assigned to GSP j ($j \in O$) and $y_{i,j}$ be an integer variable ranging from 0 to sm_{max} to indicate the entangled photon pair allocation between satellite i and GSP j. Denote $z_{p,j}$ by a binary variable to indicate whether path p ($p \in P$) is selected for GSP j for quantum swapping. We also define $\hat{y}_{p,j}$ as an integer variable ranging from 0 to sm_{max} to indicate the entangled photon pair allocation for GSP j using the path p. For any GSP $j \in O'$, if it can be served by the satellite, then we need to determine which satellite is optimal and allocate appropriate resources to this GSP j. The utility for this case can be defined as $U_1 = \sum_{j \in O'} \sum_{i \in M} w_{i,j} x_{i,j} y_{i,j}$. If no satellite can serve the GSP j, then we consider the two-hop quantum swapping by leveraging other available GSPs. Therefore, we need to determine which path is optimal and also allocate appropriate resources to the two GSPs in this path. Then, the utility for this case can be defined as $U_2 = \sum_{j \in O'} \sum_{p \in P_j} w_{p,j} z_{p,j} \hat{y}_{p,j}$.

Thus, the joint satellite assignment, resource allocation, and path selection problem is formulated as follows

$$\max_{x,y,z,\hat{y}} \sum_{j \in O'} \left(\sum_{i \in M} w_{i,j} x_{i,j} y_{i,j} + \sum_{p \in P_j} w_{p,j} z_{p,j} \hat{y}_{p,j} \right) \tag{5}$$

$$\text{s.t.} \sum_{i \in M} x_{i,j} + \sum_{p \in P_j} z_{p,j} \leq 1, \quad \forall j \in O', \tag{5a}$$

$$\sum_{i \in M} \sum_{j \in O_k} x_{i,j} \leq rr_k, \quad \forall k \in N, \tag{5b}$$

$$\sum_{j \in O} x_{i,j} \leq tr_i, \quad \forall i \in M, \tag{5c}$$

$$\sum_{i \in M} \sum_{j \in O_k} x_{i,j} y_{i,j} + \sum_{j \in O'} \sum_{\hat{j} \in O_k} \sum_{p \in P_{\hat{j}}} z_{p,j} \hat{y}_{p,j} \leq gm_k, \forall k, \tag{5d}$$

$$\sum_{j \in O'} (x_{i,j} y_{i,j} + \sum_{p \in P_i} z_{p,j} \hat{y}_{p,j}) \leq sm_i, \quad \forall i \in M, \tag{5e}$$

$$\sum_{p \in P_j} (z_{p,j} \sum_{j' \in R^{gsp}_{p,j}} \sum_{i' \in R^{sat}_{p,j}} x_{i',j'}) = (1 - \sum_{i \in M} x_{i,j}) \cdot 2, \forall j, \tag{5f}$$

$$\sum_{i \in M} x_{i,j}(F_{i,j} - F^{th}) + \sum_{p \in P_j} z_{p,j}(F_{p,j} - F^{th}) \geq 0, \forall j, \tag{5g}$$

$$x_{i,j}, z_{p,j} \in \{0,1\}, \ y_{i,j}, \hat{y}_{p,j} \in \{0, \cdots, sm_{max}\}. \tag{5h}$$

Here, constraint (5a) ensures that each GSP $j \in O'$ only connects to one satellite or only selects one swapping path if the satellite assignment is not available. Constraint (5b) means that a GS k can be part of multiple GSPs and thus is not allowed to be allocated to more than rr_k satellites. Constraint

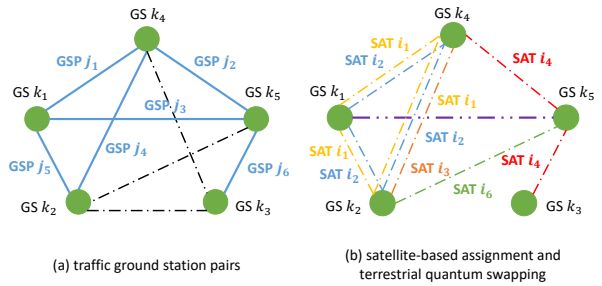

Fig. 3. Graph models of satellite-based entanglement distribution in the network of Fig. 1: (a) six traffic ground station pairs (blue lines) need quantum entanglement links in this GS graph; (b) a graph with all possible satellite-based assignment (line-dot) and terrestrial quantum swapping (line-dot-dot) for six traffic GSPs. Different colors denote different SAT candidates.

(5c) ensures that SAT i does not get allocated to more than tr_i GSPs. Constraint (5d) makes sure that the total entangled photon received from different satellites cannot exceed the maximal quantum memory of GS k. Constraint (5e) guarantees that the total entangled photon pair allocation fraction of SAT i cannot exceed sm_i. Constraint (5f) emphasizes that if a swapping path is selected, then two entanglement links along this path must be established based on the satellite assignment. Constraint (5g) confirms that the fidelity of entanglement links after transmitting or swapping is larger than the fidelity threshold. It is difficult to obtain the optimal solution to the optimization problem since this is a quadratic constrained quadratic discrete optimization problem, which is NP-hard and challenging to solve with classical computing when the problem scale increases. Note that our problem is much harder and more general than the one in [8]. Their problem is a special case of our problem (by removing quantum swapping, entangled pair allocation, and quantum memory capacity).

V. Quantum-assisted Algorithms

To tackle the complex optimization in our formulated entanglement distribution problem, we now leverage recent advanced QC to design two quantum-assisted algorithms. We first show how to convert the problem into QUBO format so that it can be solved by quantum annealer directly. Then, we introduce Dantzig-Wolfe decomposition technique [28] to break the original problem into smaller-scale problems, so that a hybrid quantum-classical solution (HQCDW) can be used to solve the optimization more efficiently.

A. Quadratic Unconstrained Binary Formulation

Inspired by the superiority of quantum annealing (QA) in solving large-scale complex optimization problems, we leverage QA to obtain the optimal solution for our joint satellite-based entanglement distribution and terrestrial quantum swapping problem in quantum networks.

To effectively solve optimization problems using the quantum annealer, these problems need to be formulated as an Ising model or a QUBO model. In a QUBO problem, there is typically a set of binary variables represented by vector $\mathbf{x}$ and an upper-diagonal matrix denoted as $\mathbf{Q}$, which is an $N' \times N'$ matrix with upper-triangular properties. The objective of QUBO is to minimize the following function:

$$f(\mathbf{x}) = \sum_i \mathbf{Q}_{i,i}\mathbf{x}_i + \sum_{i<j} \mathbf{Q}_{i,j}\mathbf{x}_i\mathbf{x}_j, \tag{6}$$

where $\mathbf{Q}_{i,i}$ is the diagonal terms with linear coefficients and $\mathbf{Q}_{i,j}$ is the nonzero off-diagonal terms with quadratic coefficients. Furthermore, (6) can be expressed as a general form defined below

$$\min_{\mathbf{x}\in\{0,1\}^{N'}} \mathbf{x}^\top \mathbf{Q}\mathbf{x}. \tag{7}$$

Note that problem (5) is a quadratic problem and all integer variables $y, \hat{y}$ can be expressed as a vector of binary variables. Hence, problem (5) can further represent the quadratic binary optimization problem. Next, we need to deal with all constraints to convert the problem into the pure QUBO form. To do so, we introduce a penalty for each constraint. The idea behind this is to find an optimal penalty coefficient of the constraints. Here, we leverage the binary search method to iteratively determine the optimal penalty for each constraint. Some constraints are converted as follows

$$(5a) \Rightarrow \quad \vartheta_1 : P^1\Big(\sum_{i\in M} x_{i,j} + \sum_{p\in P_j} z_{p,j} - 1 + \sum_{l=0}^{\bar{l}^1} 2^l s_l^1\Big)^2,$$
$$\text{where} \quad \bar{l}^1 = \lceil \log_2[1 - \min_{x,z}(\sum_{i\in M} x_{i,j} + \sum_{p\in P_j} z_{p,j})]\rceil.$$
$$\cdots$$
$$(5g) \Rightarrow \quad \vartheta_7 : P^7\Big(-\sum_{i\in M} x_{i,j}(F_{i,j} - F^{th}) - \sum_{p\in P_j} z_{p,j}(F_{p,j} - F^{th}) + \sum_{l=0}^{\bar{l}^7} 2^l s_l^7\Big)^2,$$
$$\text{where} \quad \bar{l}^7 = \lceil \log_2[\min_{x,z}(\sum_{i\in M} x_{i,j}(F_{i,j} - F^{th}) + \sum_{p\in P_j} z_{p,j}(F_{p,j} - F^{th}))]\rceil.$$

Here, P^* is the predefined penalty coefficient when the corresponding constraint is violated. s_l^* is a binary slack variable and $\bar{l}^*$ is the upper bound of the slack variable number.

Then, the original problem in (5) can be rewritten in the QUBO form as follows

$$\max_{x,y,z,\hat{y}} \quad \sum_{j\in O'} \left(\sum_{i\in M} w_{i,j}x_{i,j}y_{i,j} + \sum_{p\in P_j} w_{p,j}z_{p,j}\hat{y}_{p,j} \right) + \vartheta_1 + \vartheta_2 + \vartheta_3 + \vartheta_4 + \vartheta_5 + \vartheta_6 + \vartheta_7. \tag{8}$$

Now, we can send the reformulated problem in (8) to the quantum annealer to calculate the optimal solution. It is worth noting that the quantum annealer currently has restricted qubits and can not perform the execution when the model scale further increases. Therefore, we apply Dantzig-Wolfe decomposition to decompose the original problem into the master problem and several subproblems to reduce the model scale. In this case, the quantum annealer can solve the smaller-scale subproblems parallelly and separately.

B. Dantzig-Wolfe Decomposition

The DW decomposition algorithm is a method used to solve linear programming problems that have a specific structure (i.e., a block-angular or block-diagonal arrangement in the constraint matrix). It employs a delayed column generation (CG) technique to make solving large-scale linear programs more manageable. When applied to integer linear programming (ILP) problems, the DW algorithm often has most columns (variables) outside of the basis. The basis refers to a set of linearly independent columns from the constraint matrix that makes up the current active solution. In this approach, a master problem includes the currently active columns (basis), and a subproblem or subproblems are utilized to generate additional columns to enter the basis, thereby improving the objective function. The difference between the CG technique and DW decomposition is that in the CG process, a column is added to the master problem while an extreme point or extreme ray is added to the master problem in the DW process. In the following, we first develop an algorithm based on full linearization to reduce the non-linearity, and then we develop an improved algorithm based on partial linearization.

1) Full Linearization with Two DW subproblems: Recall that the problem in (5) is non-linear, but the DW decomposition is available to solve ILP problems. Therefore, we need to linearize the original problem first. Due to the existence of non-linear terms $x_{i,j}y_{i,j}$ and $z_{p,j}\hat{y}_{p,j}$ in the objective function and constraints, we introduce additional variables to linearize them. After full linearization, the original problem in (5) is defined as follows

$$\max_{x,y,z,\hat{y},\phi,\varphi,\psi} \quad \sum_{j\in O'}\left(\sum_{i\in M} w_{i,j}\phi_{i,j} + \sum_{p\in P_j} w_{p,j}\varphi_{p,j}\right) \tag{9}$$

s.t. $(5a)-(5h)$,

$$\phi_{i,j} \le y_{i,j}, \quad \forall i\in M, j\in O', \tag{9a}$$
$$\phi_{i,j} \le x_{i,j} sm_{max}, \quad \forall i\in M, j\in O', \tag{9b}$$
$$x_{i,j} + y_{i,j} - sm_{max} \le \phi_{i,j}, \quad \forall i\in M, j\in O', \tag{9c}$$
$$\varphi_{p,j} \le \hat{y}_{p,j}, \quad \forall j\in O', p\in P_j, \tag{9d}$$
$$\varphi_{p,j} \le z_{p,j} sm_{max}, \quad \forall j\in O', p\in P_j, \tag{9e}$$
$$z_{p,j} + \hat{y}_{p,j} - sm_{max} \le \varphi_{p,j}, \quad \forall j\in O', p\in P_j, \tag{9f}$$
$$\psi_{p,j,i',j'} \le z_{p,j}, \quad \forall j\in O', p\in P_j, i'\in R^{sat}_{p,j}, j'\in R^{gsp}_{p,j}, \tag{9g}$$
$$\psi_{p,j,i',j'} \le x_{i',j'}, \quad \forall j,p,i',j', \tag{9h}$$
$$z_{p,j} + x_{i',j'} - 1 \le \psi_{p,j,i',j'}, \quad \forall j,p,i',j', \tag{9i}$$
$$x_{i,j}, z_{p,j}, \psi_{p,j,i',j'} \in \{0,1\}, \tag{9j}$$
$$y_{i,j}, \hat{y}_{p,j}, \phi_{i,j}, \varphi_{p,j} \in \{0,\cdots,sm_{max}\}. \tag{9k}$$

Here, $\phi_{i,j}$ and $\varphi_{p,j}$ are auxiliary integer variables, $\psi_{p,j,i',j'}$ is the auxiliary binary variable. Constraints (9a)-(9c) are the linearization of non-linear term $x_{i,j}y_{i,j}$. Constraints (9d)-(9f) are the linearization of non-linear term $z_{p,j}\hat{y}_{p,j}$, while Constraints (9g)-(9i) are the linearization of non-linear term $z_{p,j}x_{i',j'}$. Since problem (9) and constraints are all linear, the problem can be further expressed as a general form below

$$\max_{\mathbf{X},\mathbf{Y}} \quad \mathbf{h}^\top\mathbf{Y} \tag{10}$$
$$\text{s.t.} \quad \mathbf{B}_1\mathbf{X} \le \mathbf{b}_1, \tag{10a}$$
$$\mathbf{B}_2\mathbf{X} = \mathbf{b}_2, \tag{10b}$$
$$\mathbf{C}\mathbf{Y} \le \mathbf{b}_3, \tag{10c}$$
$$\mathbf{A}\mathbf{X} + \mathbf{G}\mathbf{Y} \le \mathbf{b}_4, \tag{10d}$$
$$\mathbf{X} = [x,z,\psi]^\top, \quad \mathbf{X}\in\mathcal{X}, \tag{10e}$$
$$\mathbf{Y} = [y,\hat{y},\phi,\varphi]^\top, \quad \mathbf{Y}\in\mathcal{Y}, \tag{10f}$$

where $\mathbf{h}$ is the coefficient for integer variables in the objective function. $\mathbf{A}, \mathbf{B}_1, \mathbf{B}_2, \mathbf{C}$, and $\mathbf{G}$ are coefficients in the constraints while $\mathbf{b}_1$, $\mathbf{b}_2$, $\mathbf{b}_3$ and $\mathbf{b}_4$ are constant vectors. Let $dim_{\mathbf{X}} = |M|\times|O| + |P|\times|O| + |P|\times|O|\times|M|\times|O|$ and $dim_{\mathbf{Y}} = (|M|\times|O| + |P|\times|O|)\times 2$.

Next, we reformulate the original problem by increasing variable constraints to reduce the number of inequality or equality constraints. Define $\mathcal{X}$ and $\mathcal{Y}$ as

$$\mathcal{X} = \{\mathbf{X}\in\{0,1\}^{dim_{\mathbf{X}}} : \mathbf{B}_1\mathbf{X}\le\mathbf{b}_1 \text{ and } \mathbf{B}_2\mathbf{X}=\mathbf{b}_2\}, \tag{11}$$
$$\mathcal{Y} = \{\mathbf{Y}\in\{0,\cdots,sm_{max}\}^{dim_{\mathbf{Y}}} : \mathbf{C}\mathbf{Y}\le\mathbf{b}_3\}. \tag{12}$$

Then optimization problem (10) is reformulated as

$$\max_{\mathbf{X},\mathbf{Y}} \quad \mathbf{h}^\top\mathbf{Y} \tag{13}$$
$$\text{s.t.} \quad \mathbf{A}\mathbf{X} + \mathbf{G}\mathbf{Y} \le \mathbf{b}_4, \tag{13a}$$
$$\mathbf{X}\in\mathcal{X}, \tag{13b}$$
$$\mathbf{Y}\in\mathcal{Y}. \tag{13c}$$

Let $\mathcal{U}$ be the feasible region of (13). A feasible region $\mathcal{U}$ is the set of all possible points of (13) that satisfy the problem's constraints:

$$\mathcal{U} = \{\mathbf{X}\in\mathcal{X}, \mathbf{Y}\in\mathcal{Y} : \mathbf{A}\mathbf{X} + \mathbf{G}\mathbf{Y} \le \mathbf{b}_4\}. \tag{14}$$

Note that every polyhedron $\mathcal{U}$ can be written as the sum of finitely many extreme points and extreme rays. Thus, we denote its sets of extreme points with $\mathcal{P}_{\mathcal{X}} = \{\mathbf{X}^{(i)}, \forall i\in\mathcal{I}\}$ and $\mathcal{P}_{\mathcal{Y}} = \{\mathbf{Y}^{(j)}, \forall j\in\mathcal{J}\}$. Then we can express the problem (13) as the linear combination of its extreme points:

$$\max_{\substack{\mu_i,\forall i\in\mathcal{I}\\ \nu_j,\forall j\in\mathcal{J}}} \quad \sum_{j\in\mathcal{J}} (\mathbf{h}^\top\mathbf{Y}^{(j)})\nu_j \tag{15}$$
$$\text{s.t.} \quad \sum_{i\in\mathcal{I}} (\mathbf{A}\mathbf{X}^{(i)})\mu_i + \sum_{j\in\mathcal{J}} (\mathbf{G}\mathbf{Y}^{(j)})\nu_j \le \mathbf{b}_4, \tag{15a}$$
$$\sum_{i\in\mathcal{I}} \mu_i = 1, \tag{15b}$$
$$\sum_{j\in\mathcal{J}} \nu_j = 1, \tag{15c}$$
$$\mu_i \in [0,1], \quad \forall i\in\mathcal{I}, \tag{15d}$$
$$\nu_j \in [0,1], \quad \forall j\in\mathcal{J}, \tag{15e}$$

where $\mu_i \in \mathbb{R}$ and $\nu_j \in \mathbb{R}$ represent the weights of each extreme point for binary and integer variables. Since $\mathcal{I}$ and $\mathcal{J}$ contain an exponential number of extreme points, (15) will have an exponential number of variables compared to (13). Consequently, we consider a restricted version (*restricted master problem*) of (15) by progressively adding each new extreme point to the subsets $\mathcal{I}'\subseteq\mathcal{I}$ and $\mathcal{J}'\subseteq\mathcal{J}$, i.e.,

$$\max_{\substack{\mu_i,\forall i\in\mathcal{I}'\\ \nu_j,\forall j\in\mathcal{J}'}} \quad \sum_{j\in\mathcal{J}'}(\mathbf{h}^\top\mathbf{Y}^{(j)})\nu_j \tag{16}$$

$$\text{s.t.} \quad \sum_{i\in\mathcal{I}'}(\mathbf{A}\mathbf{X}^{(i)})\mu_i + \sum_{j\in\mathcal{J}'}(\mathbf{G}\mathbf{Y}^{(j)})\nu_j \le \mathbf{b}_4, \tag{16a}$$

$$\sum_{i\in\mathcal{I}'}\mu_i = 1, \tag{16b}$$

$$\sum_{j\in\mathcal{J}'}\nu_j = 1, \tag{16c}$$

$$\mu_i \in [0,1], \quad \forall i\in\mathcal{I}', \tag{16d}$$

$$\nu_j \in [0,1], \quad \forall j\in\mathcal{J}'. \tag{16e}$$

Furthermore, we introduce the Lagrangian relaxation and thus the problem can be represented as

$$\max_{\substack{\mu_i,\forall i\in\mathcal{I}'\\ \nu_j,\forall j\in\mathcal{J}'}} \quad \boldsymbol{\alpha}\mathbf{b}_4 + \sum_{i\in\mathcal{I}'}(-\boldsymbol{\alpha}\mathbf{A}\mathbf{X}^{(i)} - \xi)\mu_i + \xi + \sum_{j\in\mathcal{J}'}((\mathbf{h}^\top - \boldsymbol{\alpha}\mathbf{G})\mathbf{Y}^{(j)} - \zeta)\nu_j + \zeta, \tag{17}$$

where $\boldsymbol{\alpha}\in\mathbb{R}_+$ is the row vector (dual variable) of constraint (16a) and ξ, $\zeta\in\mathbb{R}$ are Lagrangian multipliers for constraints (16b) and (16c), respectively. Then the Lagrangian dual problem can be expressed as follows

$$\min_{\boldsymbol{\alpha},\xi,\zeta} \quad \boldsymbol{\alpha}\mathbf{b}_4 + \xi + \zeta \tag{18}$$

$$\text{s.t.} \quad -\boldsymbol{\alpha}\mathbf{A}\mathbf{X}^{(i)} - \xi \ge 0, \quad \forall i\in\mathcal{I}', \tag{18a}$$

$$(\mathbf{h}^\top - \boldsymbol{\alpha}\mathbf{G})\mathbf{Y}^{(j)} - \zeta \ge 0, \quad \forall j\in\mathcal{J}'. \tag{18b}$$

The above optimization problem is called *dual restricted master* problem. At every step t, we generate extreme points $\mathbf{X}^{(i)}$ and $\mathbf{Y}^{(j)}$. These extreme points are incorporated into the master problem, necessitating the addition of new μ_i and ν_j columns. Constraints (18a) and (18b) are called *reduced cost*. Then the two *pricing problems* (subproblems) are given as

$$\max_{\mathbf{X}\in\mathcal{X}} \quad -\boldsymbol{\alpha}^{(t)}\mathbf{A}\mathbf{X} \tag{19}$$

$$\max_{\mathbf{Y}\in\mathcal{Y}} \quad (\mathbf{h}^\top - \boldsymbol{\alpha}^{(t)}\mathbf{G})\mathbf{Y}, \tag{20}$$

where $\boldsymbol{\alpha}^{(t)}$ is the dual variables of constraint (16a). If the solution of (19) is larger than $\xi^{(t)}$, then we set $\mathcal{I}'\leftarrow\mathcal{X}^{(t)}$. Similarly, if the solution of (20) is larger than $\zeta^{(t)}$, then we set $\mathcal{J}'\leftarrow\mathcal{Y}^{(t)}$.

2) Partial Linearization with Two DW subproblems: We observe that the dimension of feasible set $\mathcal{X}$ is drastically increased with the number of SATs and GSs due to the introduced variable ψ. In addition, QUBO can handle the quadratic binary term very well. Thus, based on the DW with full linearization, we perform partial linearization where we keep the pure binary quadratic term, i.e., $x_{i,j}z_{p.j}$, and only linearize the mixed integer quadratic terms, i.e., $x_{i,j}y_{i,j}$ and $z_{p,j}\hat{y}_{p,j}$. Then the general form of problem (10) after partial linearization can be rewritten as

$$\max_{\mathbf{X},\mathbf{Y}} \quad \mathbf{h}^\top\mathbf{Y} \tag{21}$$

$$\text{s.t.} \quad \mathbf{B}_1\mathbf{X} \le \mathbf{b}_1, \tag{21a}$$

$$\mathbf{X}^\top\mathbf{B}_2\mathbf{X} = \mathbf{b}_2, \tag{21b}$$

$$\mathbf{C}\mathbf{Y} \le \mathbf{b}_3, \tag{21c}$$

$$\mathbf{A}\mathbf{X} + \mathbf{G}\mathbf{Y} \le \mathbf{b}_4, \tag{21d}$$

$$\mathbf{X} = [x,z]^\top, \quad \mathbf{X}\in\mathcal{X}, \tag{21e}$$

$$\mathbf{Y} = [y,\hat{y},\phi,\varphi]^\top, \quad \mathbf{Y}\in\mathcal{Y}, \tag{21f}$$

where the dimension of $\mathcal{X}$ is reduced to $dim_{\mathbf{X}'} = |M|\times|O| + |P|\times|O|$.

The rest of the procedure after partial linearization is similar to the one after full linearization. The only difference is that the new feasible set $\mathcal{X}$ is redefined below

$$\mathcal{X} = \{\mathbf{X}\in\{0,1\}^{dim_{\mathbf{X}'}} : \mathbf{B}_1\mathbf{X}\le\mathbf{b}_1 \text{ and } \mathbf{X}^\top\mathbf{B}_2\mathbf{X} = \mathbf{b}_2\}. \tag{22}$$

Additionally, we propose the **full and partial linearization with three DW subproblems**, where the detail can be found in Appendix A and B. With the partial linearization and three DW subproblems, the problem can be solved on a larger scale under the limited qubits in the quantum annealer.

C. Hybrid Quantum-Classical Solution: HQCDW

In this subsection, we introduce the hybrid quantum-classical algorithm for solving our original problem (5) using DW decomposition. Recall that the DW process involves solving a master problem and several subproblems iteratively. As discussed in Section V-B, the restricted master problem is defined as

$$\text{Master:} \quad \max_{\substack{\mu_i,\forall i\in\mathcal{I}'\\ \nu_j,\forall j\in\mathcal{J}'}} \quad \sum_{j\in\mathcal{J}'}(\mathbf{h}^\top\mathbf{Y}^{(j)})\nu_j \tag{23}$$

$$\text{s.t.} \quad (16a) - (16c).$$

This restricted master problem is easier to solve and can provide initial solutions for the original master problem. Hence, we can solve it by using a classical solver (e.g., Gurobi, Scipy) running in the classical CPU computer. Subsequently, two subproblems (pricing problems) are given by

$$\text{Subproblem 1:} \quad \max_{\mathbf{X}} \quad -\boldsymbol{\alpha}^{(t)}\mathbf{A}\mathbf{X} \tag{24}$$

$$\text{s.t.} \quad \mathbf{B}_1\mathbf{X} \le \mathbf{b}_1, \tag{24a}$$

$$\mathbf{B}_2\mathbf{X} = \mathbf{b}_2, \tag{24b}$$

$$\mathbf{X}\in\{0,1\}^{dim_{\mathbf{X}}}. \tag{24c}$$

$$\text{Subproblem 2:} \quad \max_{\mathbf{Y}} \quad (\mathbf{h}^\top - \boldsymbol{\alpha}^{(t)}\mathbf{G})\mathbf{Y} \tag{25}$$

$$\text{s.t.} \quad \mathbf{C}\mathbf{Y} \le \mathbf{b}_3, \tag{25a}$$

$$\mathbf{Y}\in\{0,\cdots,sm_{max}\}^{dim_{\mathbf{Y}}}. \tag{25b}$$

Here, Subproblems 1 and 2 are pure linear binary or integer problems, which can be conveniently mapped into the QUBO form as discussed in Section V-A, and we can solve them by

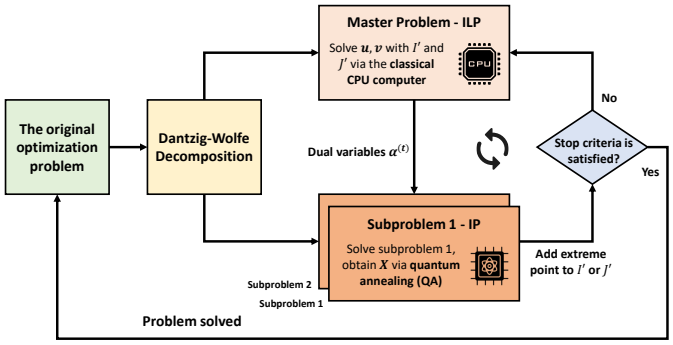

Fig. 4. HQCDW framework with two subproblems for joint satellite-based quantum entanglement distribution and terrestrial quantum swapping.

using the quantum annealer parallelly. Since the model scale of problems (24) and (25) are smaller than the original problem in (5), and they are all linear functions compared with the quadratic term in the original problem in (5), we can solve a larger-scale model compared with using pure QUBO solution. Consequently, the proposed HQCDW algorithm iteratively solves the restricted master problem and the pricing problems until convergence is reached. The detailed procedure and algorithm are shown in Fig. 4 and Algorithm 1, respectively.

In Algorithm 1, the input mainly consists of the network parameters (e.g., satellite and GS attributes) and other loss and noise parameters of downlink and uplink channels. The algorithm yields the following outcomes: assignment and allocation decisions $x_{i,j}$, $z_{p,j}$, $y_{i,j}$, and $\hat{y}_{p,j}$. The procedure starts by extracting the coefficients of the objective function and constraints, as well as initializing the extreme point (Lines 1 and 2). The initialized extreme points will be added to the extreme point set (Line 3). Then, we also initialize the dual values of the constraint (16a) as well as other parameters (e.g., the maximal number of iterations) (Lines 4-5). In the main loop, the algorithm computes two subproblems using the QA machine parallelly and determines their reduced costs (Lines 7-14). If both reduced costs are larger than 0, then the algorithm adds the new extreme point to the corresponding extreme point set (Lines 9 and 13). Next, the algorithm solves the master problem using the updated extreme point sets and then gets the related dual solution (Lines 15-17). The algorithm terminates (i.e., *stop_criteria_is_not_satisfied()* returns false) under the following conditions: (i) both reduced costs of two subproblems is less than 0, (ii) the number of current iteration reaches the maximal number of iterations. Finally, we extract the required decision values and return them. Such decisions will be used to control the STIN to distribute the entanglement to traffic GSPs.

Three DW subproblems The solution with three DW subproblems (HQCDW3) is similar to the one with two DW subproblems, but three subproblems need to be solved as shown below

$$\text{Master:} \max_{\substack{\mu_i,\forall i\in\mathcal{I}'\\ \nu_j,\forall j\in\mathcal{J}'\\ \omega_k,\forall k\in\mathcal{K}'}} \quad \sum_{j\in\mathcal{J}'}(\mathbf{h}_1^\top\mathbf{Y}_1^{(j)})\nu_j+\sum_{k\in\mathcal{K}'}(\mathbf{h}_2^\top\mathbf{Y}_2^{(k)})\omega_k \tag{26}$$

$$\text{s.t.} \quad (34a)-(34g).$$

Algorithm 1 Hybrid Quantum-Classical Dantzig-Wolfe Decomposition (HQCDW) Algorithm for Two Subproblems

Input: satellite set M, GS set N, GSP set O, quantum memory of the ith satellite sm_i, satellite transmitter tr_i, the maximal satellite quantum memory sm_{max}, quantum memory of the kth GS gm_k, GS receivers and transmitter rr_k, elevation angle threshold θ_e, utility $w_{i,j}, w_{p,j}$, and other loss and noise parameters.
Output: $x_{i,j}$, $z_{p,j}$, $y_{i,j}$, $\hat{y}_{p,j}$

1: Get $\mathbf{A}, \mathbf{B}_1, \mathbf{B}_2, \mathbf{C}, \mathbf{G}$, $\mathbf{b}_1$, $\mathbf{b}_2$, $\mathbf{b}_3$ and $\mathbf{b}_4$
2: $\mathbf{X}^{(0)}, \mathbf{Y}^{(0)} \leftarrow$ Initialize the extreme points
3: $\mathcal{I}', \mathcal{J}' \leftarrow \mathbf{X}^{(0)}, \mathbf{Y}^{(0)}$
4: $\alpha^{(0)}, \xi^{(0)}, \zeta^{(0)} \leftarrow$ Initialize the dual values
5: $max\_itr \leftarrow 100, t \leftarrow 0$, $s1, s2 \leftarrow 0, 0$
6: **while** stop_criteria_is_not_satisfied() **do**
7: $\quad s1, \mathbf{X}^{(t)} \leftarrow$ solve (24) with $\alpha^{(t)}$ ▷ quantum
8: $\quad$ **if** $s1 > \xi^{(t)}$ **then**
9: $\quad\quad \mathcal{I}' \leftarrow \mathbf{X}^{(t)}$ ▷ add the extreme point to set $\mathcal{I}'$
10: $\quad$ **end if**
11: $\quad s2, \mathbf{Y}^{(t)} \leftarrow$ solve (25) with $\alpha^{(t)}$ ▷ quantum
12: $\quad$ **if** $s2 > \zeta^{(t)}$ **then**
13: $\quad\quad \mathcal{J}' \leftarrow \mathbf{Y}^{(t)}$ ▷ add the extreme point to set $\mathcal{J}'$
14: $\quad$ **end if**
15: $\quad \mu, \nu \leftarrow$ solve (23) with $\mathbf{X}^{(t)}, \mathbf{Y}^{(t)}$ ▷ classical
16: $\quad t \leftarrow t+1$
17: $\quad \alpha^{(t)}, \xi^{(t)}, \zeta^{(t)} \leftarrow$ get dual solution from (23)
18: **end while**
19: $x_{i,j}$, $z_{p,j}$, $y_{i,j}$, $\hat{y}_{p,j} \leftarrow$ extract from $\mathcal{I}', \mathcal{J}'$
20: **return** $x_{i,j}$, $z_{p,j}$, $y_{i,j}$, $\hat{y}_{p,j}$

$$\text{Subproblem 1:} \max_{\mathbf{X}} \quad -\boldsymbol{\alpha}^{(t)}\mathbf{A}\mathbf{X} \tag{27}$$
$$\text{s.t.} \quad \mathbf{B}_1\mathbf{X} \le \mathbf{b}_1, \tag{27a}$$
$$\mathbf{B}_2\mathbf{X} = \mathbf{b}_2, \tag{27b}$$
$$\mathbf{X} \in \{0,1\}^{dim_{\mathbf{X}}}. \tag{27c}$$

$$\text{Subproblem 2:} \max_{\mathbf{Y}_1} \quad (\mathbf{h}_1^\top - \boldsymbol{\alpha}^{(t)}\mathbf{G}_1)\mathbf{Y}_1 \tag{28}$$
$$\text{s.t.} \quad \mathbf{C}_1\mathbf{Y}_1 \le \mathbf{b}_3, \tag{28a}$$
$$\mathbf{Y}_1 \in \{0,\cdots,sm_{max}\}^{dim_{\mathbf{Y}_1}}. \tag{28b}$$

$$\text{Subproblem 3:} \max_{\mathbf{Y}_2} \quad (\mathbf{h}_2^\top - \boldsymbol{\alpha}^{(t)}\mathbf{G}_2)\mathbf{Y}_2 \tag{29}$$
$$\text{s.t.} \quad \mathbf{C}_2\mathbf{Y}_2 \le \mathbf{b}_4, \tag{29a}$$
$$\mathbf{Y}_2 \in \{0,\cdots,sm_{max}\}^{dim_{\mathbf{Y}_2}}. \tag{29b}$$

Furthermore, the partial linearization solution of two and three DW subproblems are also similar, but the linear equality constraint needs to be changed to the quadratic constraint.

VI. Performance Evaluation

In this section, we examine the proposed quantum-assisted algorithms, namely the pure QUBO, HQCDW, and HQCDW3, through extensive simulations. These algorithms are put to the test on a hybrid D-Wave quantum processing unit (QPU) with around $5,000$ qubits accessed through the Leap quantum cloud service [34]. Due to the high cost of QPU utilization and the

developer's time constraints, we conducted several test cases that can be resolved in under 100 iterations. For the classical computation component, we employed the LP solver on a classical CPU computer equipped with an Intel(R) Core(TM) i7-6700HQ CPU running at 2.60 GHz and 16GB of RAM.

A. Experiment Setup

Network architecture. We consider a polar satellite constellation as discussed in [7], [8] where there are 10 spaced rings of satellites in polar orbits and 10 satellites are deployed in each ring within an altitude of 2,000 *km* to 10,000 *km*. We consider a static scenario where a few satellites are visible to a specific ground station within a fixed time window. Hence, other satellite constellations can be applied. For each satellite, the quantum memory and the number of transmitters are randomly picked from the range of $[20, 100]$ and $[6, 10]$, respectively. Furthermore, we consider several long-distance cities as GS: New York, London, Rio de Janeiro, Mumbai, Cape Town, Beijing, Sydney, Singapore, and Vancouver, where their location is based on real GPS coordinates. In this case, the maximal number of GSP $|O|$ is 36 and we randomly pick several GSPs as traffic GSPs. For each GS, the quantum memory and the number of receivers are randomly picked from the range of $[10, 20]$ and $[2, 6]$, respectively. Hereafter, we use the numbers of SATs and GSs used in experiments to represent the scale of different settings. For example, 14-5 means a test case (setting) with 14 SATs and 5 GSs.

Loss and noise parameters. For the loss and noise parameters in the transmission of photons from satellites to GS, we set them according to previous works [7], [8]: the atmospheric extinction coefficient $\alpha = 0.028125$ and the wavelength $\lambda = 737$ *nm*. In addition, we set the elevation angle threshold for any satellite and GSP $\theta_e = 10$, the transmitter telescope diameter at satellites $d_i^T = 0.2$ *m*, and the receiver telescope diameter at GSs $d_k^R = 2$ *m*.

Comparison methods. To verify the effectiveness and advantage of our algorithms, we compare our methods (pure QUBO, HQCDW, HQCDW3) with the following schemes:

- *Steepest Descent (SD)* [34]: SD is a solver for binary quadratic models provided by D-Wave Systems and the best move is computed using a local minimization.
- *Random Steepest Descent (RASD)* [34]: RASD is the combination of random sampling and steepest decent, where the algorithm performs a random sampling and a feasible result will be the input of initial states of SD.
- *Classical Optimizer (COPT)*: COPT solves the original problem (5) by using a classical optimizer (e.g., Gurobi, Scipy) in a classical CPU computer.
- *Classical DW Decomposition (CDWD)*: CDWD decouples the original problem by using DW decomposition and solves the master problem as well as all subproblems by leveraging a classical optimizer.

B. Experiment Results and Analysis

1) Performance of Number of Samples: In this part, we explore how the number of samples affects the performance of a quantum annealer in solving a problem. The number of samples represents the output solutions from the quantum annealer. The results, depicted in Fig. 5(a), compare the algorithms COPT and various QUBO variants with different sample numbers (1, 20, 50, 100, and 200) under different network settings. Across network settings, COPT consistently yields higher QUBO objective values compared to all QUBO variations. As the network complexity increases, QUBO with more samples shows higher QUBO objective values, with QUBO-200 achieving the highest values, followed by QUBO-100. QUBO-1 consistently produces the lowest values, indicating that a single sample is insufficient for good optimization results. The trend holds across all network settings, with QUBO approaching COPT's performance with a sufficient number of samples (usually 200 or more).

2) Performance in Objective Value: We proceed by comparing the performance of all methods based on the objective value. Initially, we present the objective value under various network settings using full linearization. Furthermore, for a fair comparison in terms of the quantum computation aspect for QUBO and HQCDW, we set the number of samples to 200. The results are depicted in Fig. 5(b). Firstly, SD and RASD exhibit the poorest performance across all network settings compared to the other four methods, possibly due to the SD method becoming trapped in local optima. Secondly, COPT, CDWD, QUBO-200, and HQCDW-200 achieve similar results across most network settings, except for settings 13-5 and 14-5. However, as the problem scale exceeds setting 12-5, QUBO-200 struggles to provide a solution due to the limited number of qubits in the quantum annealer. In contrast, HQCDW-200 can continue solving problems up to setting 14-5. This observation underscores the efficiency and robustness of leveraging the DW decomposition to decouple the original problem for handling larger network scales.

We then present the objective value under different network settings with three DW subproblems using partial linearization. In this case, the problem scale is increased up to setting 16-6 and we compare four DW decomposition variants, i.e., CDWD, CDWD3, HQCDW-200, and HQCDW3-200. CDWD and HQCDW-200 decompose the original problem into two subproblems, while CDWD3 and HQCDW3-200 decompose the original problem into three subproblems. The result can be found in Fig. 5(c). Similarly, SD and RASD get the worst performance among all network settings but can solve the problem scale up to 16-6. When the problem scale is beyond setting 14-5, HQCDW-200 cannot solve the problem due to the qubit limitation in solving the master problem. However, CDWD, CDWD3, and HQCDW3-200 can continue to solve the problem, which shows the advance of decomposing the original problem into more subproblems within reason. The performance difference between CDWD, CDWD3, and HQCDW3-200 lies in the solver accessing time which will be discussed later.

3) Performance in Solver Accessing Time: In this part, we investigate the performance of our proposed methods regarding the solver accessing time. The solver accessing time refers to the actual time taken by the QPU solver and local solver, excluding other overheads such as variable setting time and parameter transmission time. Initially, we compare the solver accessing time under various network settings for COPT

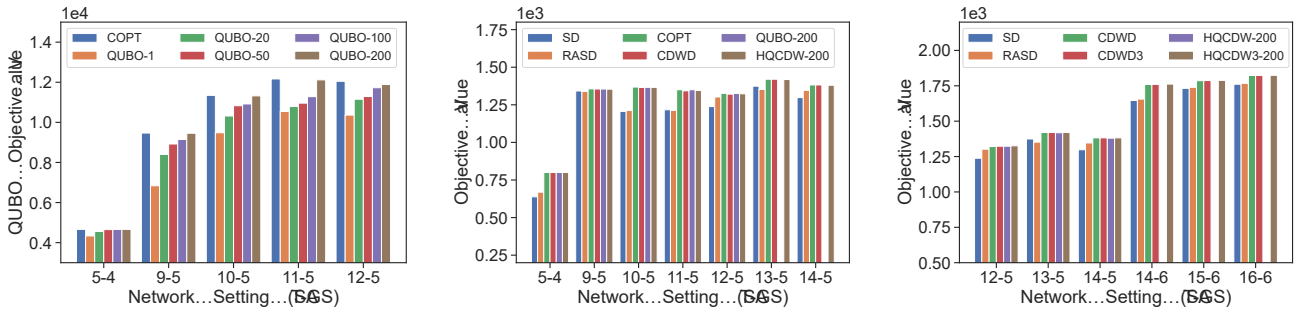

(a) The QUBO objective value (b) obj. value of two subproblems (c) obj. value of three subproblems

Fig. 5. (a) The QUBO objective value (i.e., problem (8)) under different network settings for COPT and different numbers of QUBO sampling. (b) The objective value (i.e., problem (5)) under different network settings with two DW subproblems (linear). (c) The objective value (i.e., problem (5)) under different network settings with three DW subproblems (partial-linear).

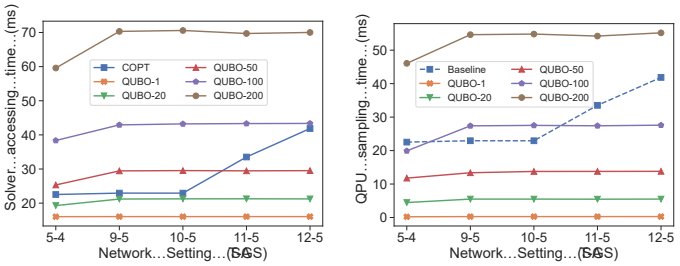

(a) solver accessing time (b) QPU sampling time

Fig. 6. (a) The solver accessing time under various network settings (from 5-4 to 12-5) for COPT and different numbers of QUBO sampling. (b) The QPU sampling time under various network settings for different numbers of QUBO sampling.

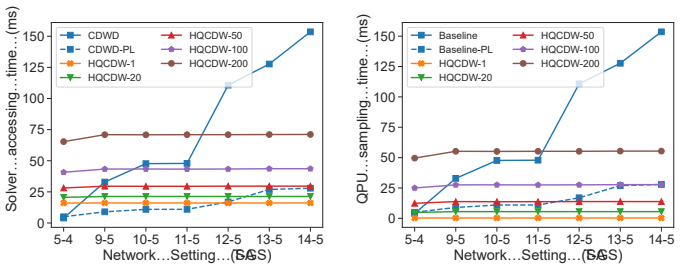

(a) solver accessing time (b) QPU sampling time

Fig. 7. (a) The solver accessing time under various network settings for CDWD-L, CDWD-PL, and different numbers of HQCDW sampling using partial linearization. (b) The QPU sampling time under various network settings for different numbers of HQCDW sampling using partial linearization.

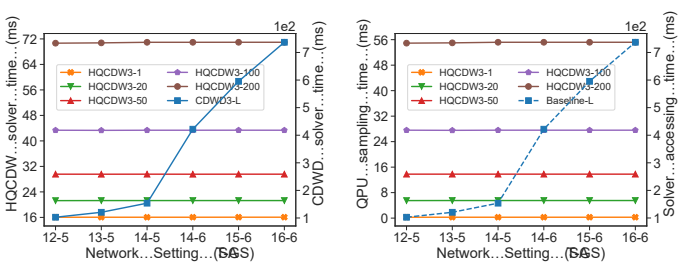

(a) solver accessing time (b) QPU sampling time

Fig. 8. (a) The solver accessing time under different network settings for CDWD3-L and different numbers of HQCDW3 sampling using full linearization. (b) The QPU sampling time under different network settings for different numbers of HQCDW3 sampling using partial linearization.

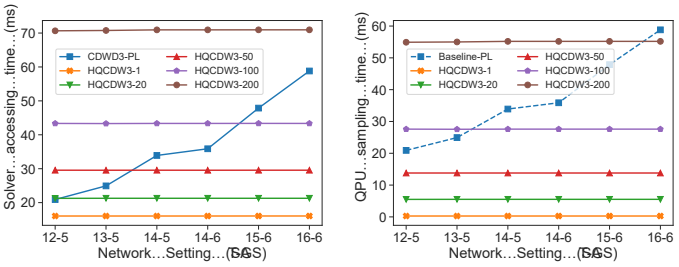

(a) solver accessing time (b) QPU sampling time

Fig. 9. (a) The solver accessing time under different network settings for CDWD3-PL and different numbers of HQCDW3 sampling using partial linearization. (b) The QPU sampling time under different network settings for different numbers of HQCDW3 sampling using partial linearization.

and different numbers of QUBO sampling, as depicted in Fig. 6(a). We can find that COPT shows a gradual increase in solver accessing time as the network setting changes from 5-4 to 12-5. QUBO-1 and QUBO-20 remain fairly consistent across different network settings, having the lowest solver accessing times. QUBO-50, QUBO-100, and QUBO-200 show an increasing trend in solver accessing time as the complexity of network settings increases, with QUBO-200 having the highest solver accessing time in each configuration. Although QUBO-200 has the highest solver accessing time, the QUBO objective value is the best among all other QUBO variants as shown in Fig. 5(a). Furthermore, COPT appears to outperform all QUBO variants when the problem scale is small. However, it is anticipated that the solver accessing time of COPT will increase significantly based on the complexity of the network setting. We further look into the specific QPU sampling time for all QUBO variants, as illustrated in Fig. 6(b). The QPU sampling time represents the total time taken to read a batch of samples from the QPU, excluding variable encoding. We observe that the overall QPU sampling time trend of all QUBO variants aligns with the solver accessing time trend but at a lower level. Furthermore, we find that all QUBO variants, except for QUBO-200, outperform the baseline (i.e., COPT).

We then analyze the solver accessing time across various network settings for CDWD-L, CDWD-PL, and different numbers of HQCDW sampling using partial linearization. The detailed comparison is presented in Fig. 7(a). Notably, CDWD-L with full linearization exhibits a significant increase in solver

accessing time as the network setting progresses from 5-4 to 14-5. Particularly for network settings beyond 11-5, the solver accessing time of CDWD-L surpasses that of HQCDW-200. Conversely, CDWD-PL with partial linearization demonstrates a gradual increase, while all HQCDW variants maintain consistency across different network settings. Furthermore, the problem can be solved up to 14-5, compared to 12-5 without leveraging the DW decomposition. A similar trend is observed for the QPU sampling time, as depicted in Fig. 7(b). This observation not only underscores the benefits of employing partial linearization to address the master problem's bottleneck but also subtly highlights the advantages of using the DW decomposition to overcome the constraints imposed by the maximum number of qubits in the quantum machine.

Next, we further demonstrate the performance of using three DW subproblems under full and partial linearization. Fig.8 shows the solver accessing time and QPU sampling time for CDWD3-L with full linearization and all HQCDW3 variants with partial linearization, while the partial linearization results of CDWD3-PL is illustrated in Fig.9. It can be seen in Fig.8 that CDWD3-L shows a significant increase in solver accessing time as the network setting changes from 12-5 to 16-6 compared to all HQCDW3 variants with a consistent time. This result further proves the efficiency and robustness of leveraging quantum annealing to solve the subproblems. Fig.9 demonstrates a similar trend as shown in Fig.7 and can solve the problem scale up to 16-6. It also reveals the importance of decomposing the original problem into a proper number of subproblems based on the problem structure. In addition, as the complexity of the network setting increases, the gap between CDWD3-PL and HQCDW-200 becomes small. From Fig.9(b), we are looking forward to a better performance of hybrid quantum-classical computing in terms of the solver accessing time and QPU sampling time.

4) Qubit Usage Comparison: We proceed to compare the total qubit usage under different network settings for two DW subproblems. In Table I, we present a comprehensive comparison of the total qubit usage across various settings, each represented as a row with size specifications such as 5-4, 9-5, 10-5, and so on. The table columns are divided into two main categories: Non-DW and DW. Non-DW denotes that the original problem is not decomposed, while DW signifies that the original problem is decomposed into two DW subproblems. Furthermore, each category is further segmented into subcategories: Quadratic (representing the original problem), Linear (indicating the full linearization of the original problem), and P-Linear (denoting the partial linearization of the original problem) for Non-DW; and Linear and P-Linear for DW. Within these subcategories, the qubit usage is further delineated into LQ (Logic Qubit used to represent the problem) and RQ (Real Qubit utilized in the quantum annealer).

Firstly, we examine the impact of problem linearization on qubit usage. Table I illustrates that the total qubit usage for both LQ and RQ increases as the network setting grows larger. This is logical, as larger problems require more qubits for representation and encoding in the quantum machine. Among the subcategories, Linear requires the most qubits, followed by P-Linear, while Quadratic uses the fewest qubits to encode the problem. This is because Linear fully linearizes all quadratic terms into linear ones, necessitating the most qubits, while P-Linear only partially linearizes some quadratic terms. Since the quantum annealer can effectively handle quadratic terms, Quadratic can encode the problem using the fewest qubits compared to Linear and P-Linear. An interesting observation is that the number of LQ and RQ is equal in Linear, while it differs in Quadratic and P-Linear. This is because the problem becomes purely an integer problem after full linearization, allowing it to be formulated as a QUBO model using the same logical qubits and real qubits. However, Quadratic and P-Linear still contain quadratic terms that require more qubits for encoding into the real quantum machine. Lastly, the Non-DW approach is limited to a network setting of 12-5, as it has utilized most of the available qubits in the quantum machine and cannot handle problem scales beyond this network setting.

Furthermore, we analyze the impact of linearization on qubit usage for the two DW subproblems. As depicted in Table I, the primary distinction lies in the linearization of subproblem X, while subproblem Y remains unchanged in Linear and P-Linear. The qubit usage of Sub Y takes precedence in the quantum machine, becoming the bottleneck in problem-solving. In P-Linear, the qubit usage of Sub X is lower than in Linear, as the quadratic term can be represented or encoded using fewer qubits compared to full linearization, which introduces additional integer variables. Similarly, the number of RQ remains larger than LQ for Sub X in P-Linear. Additionally, the DW decomposition allows us to solve larger-scale problems up to 14-5 compared to Non-DW. However, beyond the network setting of 14-5 (e.g., 14-6), the problem becomes unsolvable. This is due to the significant number of variables in the master problem, rendering it unsolvable using a classical solver. Furthermore, the qubit usage of the subproblem exceeds the maximum number of qubits in the quantum machine. Overall, the experimental data demonstrates the advantage of employing DW decomposition to solve larger-scale problems.

Lastly, we investigate the impact of the number of decomposed subproblems when using the DW decomposition technique. In this part, we decompose the original problem into three subproblems rather than two, and Table II demonstrates the result. For the case Linear, we can observe that the total qubit usage of Sub X stays the same as in two DW subproblems, while the total qubit usage of Sub Y1 and Y2 is fewer than SUB Y in two DW subproblems. Nevertheless, the solvable problem scale is also limited to 14-5 due to the limitation of the classical solver in solving the master problem. If the classical solver can overcome the limitation of maximal numbers of variables, it is believed that our methods can solve larger-scale problems. Next, we look into the performance of the partially linearized way in three DW subproblems. We also fully linearize subproblems Y1 and Y2, while subproblem X keeps the quadratic terms. There is no doubt that the total qubit usage of Sub Y1 and Y2 stays the same as in Linear, and the number of used qubits for Sub X is fewer than that in Linear. We then observe that the problem can be solved up to network setting 16-6 after partially linearizing Sub X. It can be illustrated that the linearization of Sub

TABLE I
TOTAL QUBITS USAGE UNDER DIFFERENT NETWORK SETTINGS FOR TWO DW SUBPROBLEMS.

Setting	Non-DW						DW							
	Quadratic		Linear		P-Linear		Linear				P-Linear			
							Sub X		Sub Y		Sub X		Sub Y	
	LQ	RQ	LQ	RQ	LQ	RQ	LQ	RQ	LQ	RQ	LQ	RQ	LQ	RQ
5-4	336	399	670	670	614	621	100	100	570	570	44	47	570	570
9-5	1750	2083	2856	2856	2670	2709	324	324	2532	2532	138	182	2532	2532
10-5	1960	2278	3149	3149	2943	3009	359	359	2790	2790	153	189	2790	2790
11-5	2170	2490	3484	3484	3258	3310	394	394	3090	3090	168	213	3090	3090
12-5	3360	4549	5176	5176	4820	4981	568	568	4608	4608	212	360	4608	4608
13-5	-	-	-	-	-	-	638	638	5058	5058	234	372	5058	5058
14-5	-	-	-	-	-	-	708	708	5574	5574	256	401	5574	5574

LQ: Logic Qubit, RQ: Real Qubit, "-": Not available.

TABLE II
TOTAL QUBITS USAGE UNDER DIFFERENT NETWORK SETTINGS FOR THREE DW SUBPROBLEMS.

Setting	Linear						P-Linear					
	Sub X		Sub Y1		Sub Y2		Sub X		Sub Y1		Sub Y2	
	LQ	RQ	LQ	RQ	LQ	RQ	LQ	RQ	LQ	RQ	LQ	RQ
5-4	100	100	270	270	192	192	44	47	270	270	192	192
9-5	324	324	810	810	1248	1248	138	170	810	810	1248	1248
10-5	359	359	900	900	1398	1398	153	197	900	900	1398	1398
11-5	394	394	990	990	1548	1548	168	223	990	990	1548	1548
12-5	568	568	1080	1080	2712	2712	212	331	1080	1080	2712	2712
13-5	638	638	1170	1170	3024	3024	234	354	1170	1170	3024	3024
14-5	708	708	1260	1260	3336	3336	256	389	1260	1260	3336	3336
14-6	C	C	C	C	C	C	352	557	1764	1764	4380	4380
15-6	C	C	C	C	C	C	399	687	1890	1890	5040	5040
16-6	C	C	C	C	C	C	428	692	2016	2016	5520	5520
17-6	C	C	C	C	C	C	450	729	2142	2142	5814	-

LQ: Logic Qubit, RQ: Real Qubit, "-": Not available, C: Classical optimizer limited.

X dominates the total variables of the master problem and becomes the bottleneck of solving the master problem. In other words, if we linearize Sub X, the total variables in the master problem increase significantly and the classical solver may not handle it. Overall, we have observed the advantage of using the DW decomposition technique and a proper number of decomposed subproblems, which is beneficial to solving a larger-scale problem compared to the method without using the DW decomposition.

VII. CONCLUSION

This study explores the complexities of joint satellite assignments, resource allocation, and path selection for entanglement distribution in a space-terrestrial integrated network. By utilizing both satellite-based entanglement distribution and terrestrial quantum swapping, we tackled a challenging optimization problem. Our innovative approach, combining quantum and classical computing through the Dantzig-Wolfe decomposition technique, demonstrated the potential for effectively managing large-scale network optimization tasks and optimizing qubit utilization. Through experiments, we provided compelling evidence of the efficiency and reliability of our methods, showcasing a stable solver with consistent results and faster access times compared to classical optimizers. These findings establish a solid groundwork for future advancements.

Though our model and experiments concentrate on a particular satellite network and parameter configuration, our proposed study and findings can be further extended to other network architectures and parameters. For instance, (1) other constellations such as the Iridium or Starlink constellations can be considered; (2) instead of randomly selected parameters or the simplified free-space model, more practical parameter settings and complex channel models can be considered; (3) we focus on solving the short-term static optimization problem, while the long-term optimization with the satellite dynamic can also be investigated. We leave these topics as possible future works. In addition, we will explore distributed quantum computing by decomposing complex problems into smaller, more manageable subproblems. This approach will allow us to maximize the utilization of qubits and improve the efficiency of quantum computing systems.

APPENDIX

A. Full Linearization with Three DW Subproblems

We further find that the dimension of $\mathbf{Y}$ is also the bottleneck of solving the subproblem related to $\mathbf{Y}$ since decision $\mathbf{Y}$ is an integer variable that needs to be encoded into a binary variable while using quantum annealing. The larger the

dimension of $\mathbf{Y}$, the more qubits are used to encode. Hence, we further consider a DW decomposition with three subproblems.

Following the full linearization problem (9), we reformulate the general form (10) as follows

$$\max_{\mathbf{X},\mathbf{Y}_1,\mathbf{Y}_2} \quad \mathbf{h}_1^\top \mathbf{Y}_1 + \mathbf{h}_2^\top \mathbf{Y}_2 \tag{30}$$
$$\text{s.t.} \quad \mathbf{B}_1\mathbf{X} \le \mathbf{b}_1, \tag{30a}$$
$$\mathbf{B}_2\mathbf{X} = \mathbf{b}_2, \tag{30b}$$
$$\mathbf{C}_1\mathbf{Y}_1 \le \mathbf{b}_3, \tag{30c}$$
$$\mathbf{C}_2\mathbf{Y}_2 \le \mathbf{b}_4, \tag{30d}$$
$$\mathbf{A}\mathbf{X} + \mathbf{G}_1\mathbf{Y}_1 + \mathbf{G}_2\mathbf{Y}_2 \le \mathbf{b}_5, \tag{30e}$$
$$\mathbf{X} = [x, z, \psi]^\top, \quad \mathbf{X} \in \mathcal{X}, \tag{30f}$$
$$\mathbf{Y}_1 = [y, \phi]^\top, \quad \mathbf{Y}_1 \in \mathcal{Y}_1, \tag{30g}$$
$$\mathbf{Y}_2 = [\hat{y}, \varphi]^\top, \quad \mathbf{Y}_2 \in \mathcal{Y}_2. \tag{30h}$$

The new feasible set for $\mathbf{X}$, $\mathbf{Y}_1$ and $\mathbf{Y}_2$ are rewritten below

$$\mathcal{X} = \{\mathbf{X} \in \{0,1\}^{dim_{\mathbf{X}}} : \mathbf{B}_1\mathbf{X} \le \mathbf{b}_1 \text{ and } \mathbf{B}_2\mathbf{X} = \mathbf{b}_2\}, \tag{31}$$
$$\mathcal{Y}_1 = \{\mathbf{Y}_1 \in \{0, \cdots, sm_{max}\}^{dim_{\mathbf{Y}_1}} : \mathbf{C}_1\mathbf{Y}_1 \le \mathbf{b}_3\}, \tag{32}$$
$$\mathcal{Y}_2 = \{\mathbf{Y}_2 \in \{0, \cdots, sm_{max}\}^{dim_{\mathbf{Y}_2}} : \mathbf{C}_2\mathbf{Y}_2 \le \mathbf{b}_4\}. \tag{33}$$

Similar to the case in two DW subproblems, the problem (30) can be represented as the linear combination of its extreme points:

$$\max_{\substack{\mu_i,\forall i\in\mathcal{I}'\\ \nu_j,\forall j\in\mathcal{J}'\\ \omega_k,\forall k\in\mathcal{K}'}} \quad \sum_{j\in\mathcal{J}'}(\mathbf{h}_1^\top\mathbf{Y}_1^{(j)})\nu_j + \sum_{k\in\mathcal{K}'}(\mathbf{h}_2^\top\mathbf{Y}_2^{(k)})\omega_k \tag{34}$$
$$\text{s.t.} \quad \sum_{i\in\mathcal{I}'}(\mathbf{A}\mathbf{X}^{(i)})\mu_i + \sum_{j\in\mathcal{J}'}(\mathbf{G}_1\mathbf{Y}_1^{(j)})\nu_j + \sum_{k\in\mathcal{K}'}(\mathbf{G}_2\mathbf{Y}_2^{(k)})\omega_k \le \mathbf{b}_5, \tag{34a}$$
$$\sum_{i\in\mathcal{I}'}\mu_i = 1, \tag{34b}$$
$$\sum_{j\in\mathcal{J}'}\nu_j = 1, \tag{34c}$$
$$\sum_{k\in\mathcal{K}'}\omega_k = 1, \tag{34d}$$
$$\mu_i \in [0,1], \quad \forall i \in \mathcal{I}', \tag{34e}$$
$$\nu_j \in [0,1], \quad \forall j \in \mathcal{J}', \tag{34f}$$
$$\omega_k \in [0,1], \quad \forall k \in \mathcal{K}'. \tag{34g}$$

Then we applied the Lagrangian relaxation to reformulate the problem.

$$\max_{\substack{\mu_i,\forall i\in\mathcal{I}'\\ \nu_j,\forall j\in\mathcal{J}'\\ \omega_k,\forall k\in\mathcal{K}'}} \quad \boldsymbol{\alpha}\mathbf{b}_4 + \sum_{i\in\mathcal{I}'}(-\boldsymbol{\alpha}\mathbf{A}\mathbf{X}^{(i)} - \xi)\mu_i + \xi + \sum_{j\in\mathcal{J}'}((\mathbf{h}_1^\top - \boldsymbol{\alpha}\mathbf{G}_1)\mathbf{Y}_1^{(j)} - \zeta)\nu_j + \zeta + \sum_{k\in\mathcal{K}'}((\mathbf{h}_2^\top - \boldsymbol{\alpha}\mathbf{G}_2)\mathbf{Y}_2^{(k)} - \sigma)\omega_k + \sigma, \tag{35}$$

where $\boldsymbol{\alpha}$ is the dual variable of constraint (34a), ξ, ζ and σ are dual variable of constraints (34b), (34c) and (34d), respectively. Then the related dual problem is defined as

$$\min_{\boldsymbol{\alpha},\xi,\zeta,\sigma} \quad \boldsymbol{\alpha}\mathbf{b}_5 + \xi + \zeta + \sigma \tag{36}$$
$$\text{s.t.} \quad -\boldsymbol{\alpha}\mathbf{A}\mathbf{X}^{(i)} - \xi \ge 0, \quad \forall i \in \mathcal{I}', \tag{36a}$$
$$(\mathbf{h}_1^\top - \boldsymbol{\alpha}\mathbf{G}_1)\mathbf{Y}_1^{(j)} - \zeta \ge 0, \quad \forall j \in \mathcal{J}', \tag{36b}$$
$$(\mathbf{h}_2^\top - \boldsymbol{\alpha}\mathbf{G}_2)\mathbf{Y}_2^{(k)} - \sigma \ge 0, \quad \forall k \in \mathcal{K}'. \tag{36c}$$

At every step t in DW, at most three extreme points $\mathbf{X}^{(i)}$, $\mathbf{Y}_1^{(j)}$ and $\mathbf{Y}_2^{(k)}$ are generated and incorporated into the master problem, necessitating the addition of new μ_i, ν_j and ω_k columns. Then three subproblems are defined as

$$\max_{\mathbf{X}\in\mathcal{X}} \quad -\boldsymbol{\alpha}^{(t)}\mathbf{A}\mathbf{X}. \tag{37}$$

$$\max_{\mathbf{Y}_1\in\mathcal{Y}_1} \quad (\mathbf{h}_1^\top - \boldsymbol{\alpha}^{(t)}\mathbf{G}_1)\mathbf{Y}_1. \tag{38}$$

$$\max_{\mathbf{Y}_1\in\mathcal{Y}_2} \quad (\mathbf{h}_2^\top - \boldsymbol{\alpha}^{(t)}\mathbf{G}_2)\mathbf{Y}_2. \tag{39}$$

If the solution of (37) is larger than $\xi^{(t)}$, then we set $\mathcal{I}' \leftarrow \mathcal{X}^{(t)}$. Similarly, If the solution of (38) is larger than $\zeta^{(t)}$, then we set $\mathcal{J}' \leftarrow \mathcal{Y}_1^{(t)}$. If the solution of (39) is larger than σ^t, we set $\mathcal{K}' \leftarrow \mathcal{Y}_2^{(t)}$.

B. Partial Linearization with Three DW Subproblems

We also consider the partial linearization for binary variables, hence the constraints (30b) and (30f) need to be rewritten as follows

$$\max_{\mathbf{X},\mathbf{Y}_1,\mathbf{Y}_2} \quad \mathbf{h}_1^\top \mathbf{Y}_1 + \mathbf{h}_2^\top \mathbf{Y}_2 \tag{40}$$
$$\text{s.t.} \quad \mathbf{B}_1\mathbf{X} \le \mathbf{b}_1, \tag{40a}$$
$$\mathbf{X}^\top\mathbf{B}_2\mathbf{X} = \mathbf{b}_2, \tag{40b}$$
$$\mathbf{C}_1\mathbf{Y}_1 \le \mathbf{b}_3, \tag{40c}$$
$$\mathbf{C}_2\mathbf{Y}_2 \le \mathbf{b}_4, \tag{40d}$$
$$\mathbf{A}\mathbf{X} + \mathbf{G}_1\mathbf{Y}_1 + \mathbf{G}_2\mathbf{Y}_2 \le \mathbf{b}_5, \tag{40e}$$
$$\mathbf{X} = [x, z]^\top, \quad \mathbf{X} \in \mathcal{X}, \tag{40f}$$
$$\mathbf{Y}_1 = [y, \phi]^\top, \quad \mathbf{Y}_1 \in \mathcal{Y}_1, \tag{40g}$$
$$\mathbf{Y}_2 = [\hat{y}, \varphi]^\top, \quad \mathbf{Y}_2 \in \mathcal{Y}_2. \tag{40h}$$

Then the rest of the procedure after the partial linearization is similar to the one after full linearization with three DW subproblems.

REFERENCES

[1] T. K. Paraiso, T. Roger, D. G. Marangon, I. De Marco, *et al.*, "A photonic integrated quantum secure communication system," *Nature Photonics*, vol. 15, no. 11, pp. 850–856, Oct. 2021.

[2] P. W. Shor and J. Preskill, "Simple proof of security of the BB84 quantum key distribution protocol," *Physical review letters*, vol. 85, no. 2, pp. 441–444, Jul. 2000.

[3] J.-G. Ren, P. Xu, H.-L. Yong, *et al.*, "Ground-to-satellite quantum teleportation," *Nature*, vol. 549, no. 7670, pp. 70–73, Aug. 2017.

[4] J. Yin, Y. Cao, Y.-H. Li, S.-K. Liao, L. Zhang, J.-G. Ren, W.-Q. Cai, W.-Y. Liu, B. Li *et al.*, "Satellite-based entanglement distribution over 1200 kilometers," *Science*, vol. 356, no. 6343, pp. 1140–1144, Jun. 2017.

[5] Z. Wang, R. Malaney, and J. Green, "Satellite-based entanglement distribution using orbital angular momentum of light," in *Proc. of IEEE INFOCOM Workshops*, 2020.
[6] J. Yin, Y.-H. Li, S.-K. Liao, M. Yang, Y. Cao, L. Zhang, *et al.*, "Entanglement-based secure quantum cryptography over 1,120 kilometres," *Nature*, vol. 582, no. 7813, pp. 501–505, Jun. 2020.
[7] S. Khatri, A. J. Brady, R. A. Desporte, M. P. Bart, and J. P. Dowling, "Spooky action at a global distance: analysis of space-based entanglement distribution for the quantum Internet," *npj Quantum Information*, vol. 7, no. 4, pp. 1–15, Jan. 2021.
[8] N. K. Panigrahy, P. Dhara, D. Towsley, S. Guha, and L. Tassiulas, "Optimal entanglement distribution using satellite based quantum networks," in *Proc. of IEEE INFOCOM Workshops*, 2022.
[9] X. Wei, J. Liu, L. Fan, Y. Guo, Z. Han, and Y. Wang, "Optimal entanglement distribution problem in satellite-based quantum networks," *IEEE Network*, 2024.
[10] X. Wei, L. Fan, Y. Guo, Z. Han, and Y. Wang, "Optimizing satellite-based entanglement distribution in quantum networks via quantum-assisted approaches," in *Proc. of IEEE QCNC*, 2024.
[11] J. Yin, J.-G. Ren, H. Lu, Y. Cao, *et al.*, "Quantum teleportation and entanglement distribution over 100-kilometre free-space channels," *Nature*, vol. 488, no. 7410, pp. 185–188, Aug. 2012.
[12] C. Liorni, H. Kampermann, and D. Bruß, "Quantum repeaters in space," *New Journal of Physics*, vol. 23, no. 053021, pp. 1–15, May 2021.
[13] T. Gonzalez-Raya, S. Pirandola, and M. Sanz, "Satellite-based entanglement distribution and quantum teleportation with continuous variables," *arXiv preprint arXiv:2303.17224*, Mar. 2023.
[14] A. Chang, Y. Wan, G. Xue, and A. Sen, "Entanglement distribution in satellite-based dynamic quantum networks," *IEEE Network*, vol. 38, no. 1, pp. 79–86, Jan. 2024.
[15] Y.-W. Jeong, J.-B. Park, S.-H. Jang, and K. Y. Lee, "A new quantum-inspired binary PSO: Application to unit commitment problems for power systems," *IEEE Transactions on Power Systems*, vol. 25, no. 3, pp. 1486–1495, Aug. 2010.
[16] F. Glover, G. Kochenberger, and Y. Du, "Quantum bridge analytics i: a tutorial on formulating and using qubo models," *Annals of Operations Research*, vol. 17, pp. 335–371, Apr. 2022.
[17] A. Ajagekar and F. You, "Quantum computing for energy systems optimization: Challenges and opportunities," *Energy*, vol. 179, pp. 76–89, Jul. 2019.
[18] W. A. Borders, A. Z. Pervaiz, S. Fukami, K. Y. Camsari, H. Ohno, and S. Datta, "Integer factorization using stochastic magnetic tunnel junctions," *Nature*, vol. 573, no. 7774, pp. 390–393, Sep. 2019.
[19] J. Tilly, H. Chen, S. Cao, D. Picozzi, K. Setia, Y. Li, E. Grant, L. Wossnig, I. Rungger, G. H. Booth *et al.*, "The variational quantum eigensolver: a review of methods and best practices," *Physics Reports*, vol. 986, pp. 1–128, Nov. 2022.
[20] T. Tran, M. Do, E. Rieffel, J. Frank, Z. Wang, B. O'Gorman, D. Venturelli, and J. Beck, "A hybrid quantum-classical approach to solving scheduling problems," in *Proceedings of the International Symposium on Combinatorial Search*, New York, NY, Jul. 2016.
[21] A. Ajagekar, T. Humble, and F. You, "Quantum computing based hybrid solution strategies for large-scale discrete-continuous optimization problems," *Computers & Chemical Engineering*, vol. 132, no. 106630, pp. 1–19, Jan. 2020.
[22] N. G. Paterakis, "Hybrid quantum-classical multi-cut benders approach with a power system application," *Computers & Chemical Engineering*, vol. 172, no. 108161, pp. 1–17, Apr. 2023.
[23] Z. Zhao, L. Fan, and Z. Han, "Hybrid quantum benders' decomposition for mixed-integer linear programming," in *Proc. of IEEE WCNC*, 2022.
[24] A. Ajagekar, K. Al Hamoud, and F. You, "Hybrid classical-quantum optimization techniques for solving mixed-integer programming problems in production scheduling," *IEEE Transactions on Quantum Engineering*, vol. 3, pp. 1–16, Jun. 2022.
[25] L. Fan and Z. Han, "Hybrid quantum-classical computing for future network optimization," *IEEE Network*, vol. 36, no. 5, pp. 72–76, Nov. 2022.
[26] Z. Zhao, L. Fan, Y. Guo, Y. Wang, Z. Han, and L. Hanzo, "QAOA-assisted benders' decomposition for mixed-integer linear programming," in *Proc. of IEEE ICC*, 2024.
[27] X. Wei, L. Fan, Y. Guo, Y. Gong, Z. Han, and Y. Wang, "Quantum assisted scheduling algorithm for federated learning in distributed networks," in *Proc. of IEEE ICCCN*, 2023.
[28] X. Wei, J. Liu, L. Fan, Y. Guo, Z. Han, and Y. Wang, "Hybrid quantum-classical computing via dantzig-wolfe decomposition for integer linear programming," in *Proc. of IEEE ICCCN*, 2024.
[29] X. Wei, L. Fan, Y. Guo, Y. Gong, Z. Han, and Y. Wang, "Hybrid quantum-classical benders' decomposition for federated learning scheduling in distributed networks," *IEEE Transactions on Network Science and Engineering*, 2024.
[30] P. Dhara, S. J. Johnson, C. N. Gagatsos, P. G. Kwiat, and S. Guha, "Heralded multiplexed high-efficiency cascaded source of dual-rail entangled photon pairs using spontaneous parametric down-conversion," *Physical Review Applied*, vol. 17, no. 034071, pp. 1–24, Mar. 2022.
[31] H. Gu, Z. Li, R. Yu, X. Wang, F. Zhou, and J. Liu, "Fendi: High-fidelity entanglement distribution in the quantum Internet," *arXiv preprint arXiv:2301.08269*, Jan. 2023.
[32] N. K. Panigrahy, T. Vasantam, D. Towsley, and L. Tassiulas, "On the capacity region of a quantum switch with entanglement purification," *arXiv preprint arXiv:2212.01463*, Dec. 2022.
[33] A. Zang, X. Chen, A. Kolar, and J. Chung, "Entanglement distribution in quantum repeater with purification and optimized buffer time," in *Proceedings of IEEE INFOCOM Workshops*, 2023.
[34] D-Wave Systems Inc., "Ocean software documentation: dwave-samplers, steepestdescentsolver, randomsampler," Oct. 2023. [Online]. Available: https://docs.ocean.dwavesys.com/en/stable/docs_samplers/reference.html

Xinliang Wei (S'21-M'23) holds a Ph.D. in Computer and Information Sciences from Temple University, Philadelphia, USA in 2023. He received his M.S. and B.E. degrees both in Software Engineering from SUN Yat-sen University, Guangzhou, China in 2016 and 2014, respectively. His research interests include edge computing, federated learning, reinforcement learning, and Internet of Things. He is a recipient of *Outstanding Research Assistant* from College of Science and Technology (2022) and *Scott Hibbs Future of Computing Award* from Department of Computer & Information Sciences (2023) at Temple University. He is currently an Assistant Professor in Shenzhen Institute of Advanced Technology, Chinese Academy of Sciences.

Lei Fan (M'15-SM'20) is an Assistant Professor in the Department of Engineering Technology as well as in the Department of Electrical and Computer Engineering at University of Houston. Before this position, he worked in the electricity energy industry for several years. He received the Ph.D. degree in operations research from the Industrial and System Engineering Department at University of Florida. His research includes quantum computing, optimization methods, complex system operations, power system operations and planning.

Yuanxiong Guo (M'14-SM'19) received the B.Eng. degree in electronics and information engineering from the Huazhong University of Science and Technology, China, in 2009, and the M.S. and Ph.D. degrees in electrical and computer engineering from the University of Florida, in 2012 and 2014, respectively. He is currently an Associate Professor in the Department of Information Systems and Cyber Security at the University of Texas at San Antonio. His current research interests include distributed machine learning, applied data science, and trustworthy AI with application to digital health, energy sustainability, and human-robot collaboration. He is on the Editorial Board of IEEE Transactions on Vehicular Technology and servers as the track co-chair for IEEE VTC 2021-Fall. He is a recipient of the Best Paper Award in the IEEE GLBOECOM 2011.

Zhu Han (S'01-M'04-SM'09-F'14) received the B.S. degree in electronic engineering from Tsinghua University, in 1997, and the M.S. and Ph.D. degrees in electrical and computer engineering from the University of Maryland, College Park, in 1999 and 2003, respectively. Currently, he is a John and Rebecca Moores Professor in the Electrical and Computer Engineering Department as well as in the Computer Science Department at the University of Houston, Texas. His research interests include game theory, wireless resource allocation and management, wireless communications and networking, quantum computing, data science, smart grid, carbon neutralization, security and privacy. He received an NSF Career Award in 2010, the Fred W. Ellersick Prize of the IEEE Communication Society in 2011, the EURASIP Best Paper Award for the Journal on Advances in Signal Processing in 2015, IEEE Leonard G. Abraham Prize in the field of Communications Systems in 2016, IEEE Vehicular Technology Society 2022 Best Land Transportation Paper Award, 2021 IEEE Kiyo Tomiyasu Award, and several best paper awards in IEEE conferences. Dr. Han was an IEEE Communications Society Distinguished Lecturer from 2015 to 2018 and ACM Distinguished Speaker from 2022 to 2025, AAAS fellow since 2019, and ACM Fellow since 2024. Dr. Han is a 1% highly cited researcher since 2017 according to Web of Science.

Yu Wang (S'02-M'04-SM'10-F'18) is a Professor and Chair of the Department of Computer and Information Sciences at Temple University. He holds a Ph.D. from Illinois Institute of Technology, an MEng and a BEng from Tsinghua University, all in Computer Science. His research interest includes wireless networks, smart sensing, and distributed computing. He is a recipient of *Ralph E. Powe Junior Faculty Enhancement Awards* from Oak Ridge Associated Universities (2006), *CCI Outstanding Faculty Research Award* from the University of North Carolina at Charlotte (2008), *Fellow of IEEE* (2018), *ACM Distinguished Member* (2020), and *IEEE Benjamin Franklin Key Award* (2024). He has served as Associate Editor for *IEEE Transactions on Parallel and Distributed Systems*, *IEEE Transactions on Cloud Computing*, among others.